Inorganic Chemistry

Article

pubs.acs.org/IC

Density Functional Theory Calculations of UO_2 Oxidation: Evolution of UO_{2+x}, U_4O_{9-y}, U_3O_7, and U_3O_8

D. A. Andersson,*[,†] G. Baldinozzi,[‡] L. Desgranges,[§] D. R. Conradson,[†] and S. D. Conradson[†]

[†]Materials Science and Technology Division, Los Alamos National Laboratory, Los Alamos, New Mexico 87545, United States

[‡]SPMS, LRC Carmen, CNRS Ecole Centrale Paris, Châtenay-Malabry, France

[§]CEA/DEN/DEC, Centre de Cadarache, Saint-Paul-lez-Durance, France

Supporting Information

ABSTRACT: Formation of hyperstoichiometric uranium dioxide, UO_{2+x}, derived from the fluorite structure was investigated by means of density functional theory (DFT) calculations. Oxidation was modeled by adding oxygen atoms to UO_2 fluorite supercells. For each compound ab initio molecular dynamics simulations were performed to allow the ions to optimize their local geometry. A similar approach was used for studying the reduction of U_3O_8. In agreement with the experimental phase diagram we identify stable line compounds at the U_4O_{9-y} and U_3O_7 stoichiometries. Although the transition from fluorite to the layered U_3O_8 structure occurs at U_3O_7 ($UO_{2.333}$) or $U_3O_{7.333}$ ($UO_{2.444}$), our calculated low temperature phase diagram indicates that the fluorite derived compounds are favored up to $UO_{2.5}$, that is, as long as the charge-compensation for adding oxygen atoms occurs via formation of U^{5+} ions, after which the U_3O_{8-y} phase becomes more stable. The most stable fluorite UO_{2+x} phases at low temperature (0 K) are based on ordering of split quad-interstitial oxygen clusters. Most existing crystallographic models of U_4O_9 and U_3O_7, however, apply the cuboctahedral cluster. To better understand these discrepancies, the new structural models are analyzed in terms of existing neutron diffraction data. DFT calculations were also performed on the experimental cuboctahedral based U_4O_{9-y} structure, which enable comparisons between the properties of this phase with the quad-interstitial ones in detail.

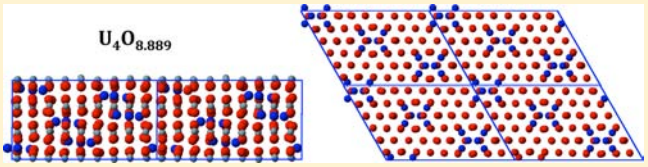

1. INTRODUCTION

Oxidation of UO_2 is important for processes involved in nuclear fuel fabrication and handling, for understanding fuel variations during reactor operation, and for predicting the chemistry of spent fuels.[1−3] Hyperstoichiometric fluorite derived uranium dioxide (UO_{2+x}) is one of the most complex binary materials with large homogeneity fields as well as several long-range ordered compounds with large unit cells.[1,4−12] The two most stable ones are U_4O_{9-y} and U_3O_7, both of which exhibit multiple polymorphs as a function of temperature. These properties are related to the mixed valence character of uranium oxides (U exhibits stable valences of III−VI where adjacent ones easily coexist) and to the strong tendency of interstitial oxygen ions in UO_{2+x} to form clusters. Above a U:O ratio of 3/7 the fluorite structure does not accommodate more oxygen ions and transforms to U_3O_8,[1,8] which has a unique crystal structure derived from the fluorite UO_{2+x} structure via a shear transformation.[4,13]

Despite extensive study of hypervalent UO_{2+x},[1,8,10,12] there are still uncertainties regarding a number of the compound structures as well as the physics underlying the unique structures and electronic properties. This is especially true for the low-temperature phases of U_3O_7 and U_4O_9 (α-U_3O_7 and α-U_4O_9),[4,8,6,14] The most recent crystallographic models of the U_4O_9 and U_3O_7 line compounds apply the cuboctahedral oxygen cluster first proposed by Bevan et al.[7,11,14,15] Alternative models were proposed by Conradson et al. based on EXAFS measurements,[16] which in addition to the U−O bond geometries present in cuboctahedral models (≈ 2.2−2.4 Å) found contributions from much shorter U−O bonds (≈ 1.7 Å). The latter are the preferred coordination in U(VI) molecular complexes in aqueous systems where they form the trans dioxo uranyl moiety; however, they are not compatible with the fluorite lattice. Desgranges et al.[14] revealed that the ordering pattern for the low temperature α-U_4O_9 phase differed from the intermediate temperature β-U_4O_9 phase. The structure that they found involved short U−O bonds, which is the same geometry that was identified by Conradson et al.,[16] and they invoked U_3O_8 like distortions in the fluorite lattice to explain this behavior. Additional work on U_4O_9 and U_3O_7 by Conradson et al.[17] using both neutron and X-ray scattering techniques revealed differences in the pair distribution function between the two techniques. This was interpreted as a dynamic instability of the defect sites,[18] induced by valence or charge fluctuations on the uranium ions coupling to the $UO_{2+x} \leftrightarrow U_3O_8$ transformation.[13] The O vacancies could then promote the formation of the shorter U−O bonds. This is similar to the mechanism proposed by Desgranges et al.[14] Only a few attempts have been made to solve the crystal structure of U_3O_7,[6,8] of which Desgranges et al.[8] is probably the most ambitious one. All existing U_3O_7 models are extensions of the

Received: January 16, 2013
Published: February 13, 2013

   dx.doi.org/10.1021/ic400118p | Inorg. Chem. 2013, 52, 2769−2778

cuboctahedral structure model proposed for U_4O_9. Compared to U_4O_9 the most prominent feature of the U_3O_7 crystallography is a highly variable tetragonal symmetry reduction.[6,8]

Though β-U_4O_9 and α-U_4O_9 already display large departures from the UO_2 stoichiometry, the symmetry of these phases is still cubic (β phase) or pseudocubic (α phase), but with a very weak ferroelastic distortion. This suggests that the fluorite structure can efficiently accommodate large concentrations of complex atomic defects without building up significant (local) strain that usually induces large ferroelastic instabilities that might destabilize it. This is evident in the fact that the simple fluorite cell undergoes almost no change in volume across the entire composition range. Ferroelastic distortions (the emerging feature of those complex defect interactions) start becoming significant in U_3O_7. Therefore, long-range correlations between defects are essential for reproducing all the structural features in U_3O_7 but may not play a primary part in β-U_4O_9, so it makes sense to check many local configurations in this structure rather than different stackings of the same defects that are possibly a core feature in energy minimization in U_3O_7.

To gain better understanding of these processes, we have simulated the oxidation of fluorite UO_2 and the formation of U_3O_8 using density functional theory (DFT) calculations. In particular, we have considered the formation of the single phase compositions U_4O_9 and U_3O_7 and the transformation from UO_{2+x} to U_3O_8. Our study uses earlier DFT work on oxygen clustering in UO_{2+x} as its starting point.[19,20] Specifically, the "split quad-interstitial" cluster, which was found to be the most stable configuration of interstitial oxygen ions in UO_{2+x} from DFT calculations, is used as the building block of these compounds. The split quad-interstitial is composed of four adventitious and two displaced fluorite oxygen ions that can also be described as a bound state of two triangular di-interstitial clusters. We refer to refs 19, 20 for details. Other cluster types, such as the cuboctahedral cluster established from neutron diffraction experiments and containing five adventitious oxygen ions, were also explored.

The paper is organized as follows. In Section 2 we present the DFT methodology. Next we describe the different structural models used for studying the addition of oxygen atoms to UO_2 or removal from U_3O_8. In the results section (Section 4) the formation energies and atomic volumes of UO_{2+x} and U_3O_{8-y} compounds are discussed. Finally, we compare the new structures found from DFT with available neutron diffraction data.

2. METHODOLOGY

The DFT calculations used the LDA+U[21] (here also denoted as DFT+U) and projector augmented wave (PAW)[22,23] methods, as implemented in the Vienna Ab Initio Simulation Package (VASP).[24−26] The LDA+U methodology[21] improves the description of strongly correlated U 5f electrons. Other approaches to achieve this include hybrid functionals[27,28] and the self-interaction corrected local spin-density approximation.[29] In the Lichtenstein formulation of LDA+U[21] applied here, the spherically averaged screened Coulomb energy, U, and the exchange energy, J, must be specified. For UO_2, U and J parameters of 4.5 and 0.5 eV, respectively, were originally derived by Dudarev[30] based on experimental measurements and have since been widely applied.[19,30−48] Here these parameters were adopted for all UO_{2+x} compounds and for U_3O_{8-y}. The application of the U and J values derived for UO_2 to UO_{2+x} and U_3O_8 is an approximation, since the appropriate values may change slightly as function of, for example, nonstoichiometry and crystal structure. We did not attempt to independently determine separate values, for example, for U_3O_8. However, because of the structural similarities between all of these compounds we consider this approximation to be reasonable and at this point the best possible. We did verify that changing the U parameter, for example, for U_3O_7, did not drastically change the structure or the balance between U^{4+}, U^{5+}, and U^{6+} ions. Moreover, DFT calculations based on the structure models derived in this work have been shown to capture the electronic structure of UO_2, U_4O_9, and U_3O_7 measured by X-ray absorption spectroscopy (XAS) rather well.[49] This indicates that even though the present choice of U parameters for UO_{2+x} is based on simplifying assumptions it is accurate enough to support the largely qualitative conclusions derived in this work. Yun et al. performed extensive studies of U_3O_8 using the DFT+U methodology[47] and in agreement with our approach they applied U and J values in the range established for UO_2. In contrast, Geng et al. chose to use standard DFT instead of DFT+U in their study of U_3O_8.[50] For both UO_2 and U_3O_8 the localized spins on uranium ions were assumed to be ordered in an antiferromagnetic (AFM) pattern. This was obtained as the lowest energy configuration in the DFT calculations. Spin−orbit coupling and noncollinear magnetic ordering were ignored to simplify the calculations. Both volume and internal structural parameters were relaxed for all crystal structures and symmetries were unconstrained. The internal structural parameters were relaxed until the Hellmann−Feynman forces on each ion were sufficiently small (<0.02 eV/Å) or until the total energy was converged to at least 0.0001 eV/atom. The plane-wave cutoff was set to 500 eV and convergence with respect to k point meshes was verified. For the 2 × 2 × 2 UO_2 supercell containing 96 atoms we used a 2 × 2 × 2 Monkhorst-Pack k point mesh, while only the single Γ point was used for the largest UO_{2+x} ($U_4O_{8.938}$) superstructure described within a cell containing 414 atoms. Other structure models used a k point density that was at least as high as these two examples.

For UO_2 and $UO_{2\pm x}$ it has been shown that the DFT+U methodology may converge to different occupation matrices for the U 5f orbitals, which gives rise to metastable solutions.[39,41] In this work we report data for structures where all symmetries were removed, which for UO_2 is equivalent to the phase with small structural distortions from the ideal fluorite lattice. This has been described as a Jahn−Teller distortion in previous studies.[41] Although, the reduced symmetry decreases issues with metastable electronic solutions, we have also applied both the occupation matrix control scheme developed by Dorado et al.[39,41] and the U ramping method due to Meredig et al.[43] to verify that the calculated energies are as close to the lowest energy solution as possible. Despite these efforts we cannot guarantee that the minimum energy solution has been attained. Note that the higher oxides of uranium such as U_3O_8 are much less sensitive to metastable electronic solutions than UO_2 or UO_{2+x}. Current versions of the DFT+U method include self-interaction errors in the exchange term for f elements.[51] To solve this issue Zhou et al. developed a self-interaction free formulation of the DFT+U method, which gave very accurate predictions for UO_2.[52] The improved formulation was, however, not applied here.

The possibility of different charge states for the oxygen clusters was not considered. In the DFT+U framework this implies that each interstitial is compensated by two U^{5+} ions or one U^{6+} ion. The local atom projected magnetic moments were used to classify the charge or valence state of U ions.[53] Crocombette et al.[54,55] showed that charged solutions deviating from the nominal charge compensation may be favorably close to stoichiometric UO_2 for single interstitials and likely also for larger clusters. However, since we are primarily concerned with properties at higher x where the Fermi level should be close to the valence band edge[56−58] and thus favoring solutions with charge-compensating U^{5+}/U^{6+} ions, the present approach should be valid.

To explore local rearrangements of adventitious oxygen ions we have carried out ab initio molecular dynamics simulations at constant temperature and volume (NVT ensemble). The temperature (up to 1473 K) and time step (up to 5 fs) was chosen to enable transformation within the relatively short simulation times that could be reached. The simulations were run for a minimum of 250 time steps. This approach is similar to the one applied in ref 20 to study the

dx.doi.org/10.1021/ic400118p | Inorg. Chem. 2013, 52, 2769−2778

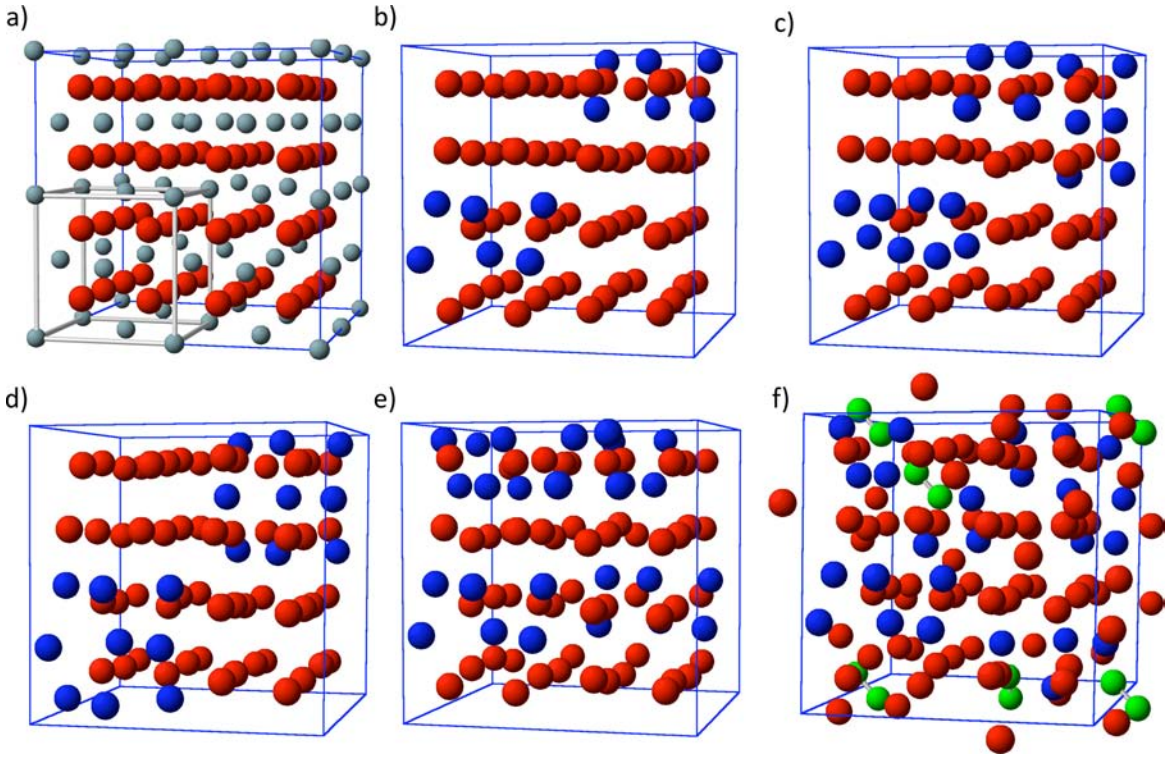

Figure 1. The 2 × 2 × 2 supercell and some of the most stable 2 × 2 × 2 structures as function of oxygen nonstoichiometry.[62] In all figures red spheres represent regular oxygen ions and gray spheres uranium ions. The cluster ions are highlighted in blue color. To improve the visibility, the uranium sublattice is not shown for (b)-(f). (a) The 2 × 2 × 2 supercell. The conventional fluorite unit cell is highlighted by bold lines. (b) Two split quad-interstitials aligned in the same direction (U_4O_9 or $UO_{2.25}$), which is labeled as U_4O_9(bcc) in the text. (c) Three split quad-interstitials ($U_4O_{9.5}$ or $UO_{2.75}$) that transformed into one split quad-intersitial, one five atom cluster (transformed cuboctahedral cluster), and one tri-interstitial cluster after annealing. (d) Two five-atom oxygen clusters corresponding to two transformed cuboctahedral clusters aligned in the same direction ($U_4O_{9.25}$ or $UO_{2.3125}$). (e) Four split quad-interstitials of which two are aligned in the same direction and the other two clusters are orthogonal to the first two (U_4O_{10} or $UO_{2.5}$). (f) Five split quad-interstitials ($U_4O_{10.5}$ or $UO_{2.625}$). In this case the view is expanded beyond a single supercell to better visualize the peroxide ions located at the supercell edges (shown in green and the corresponding ≈ 1.4 Å bonds are also included).

relation between different oxygen clusters in UO_{2+x}. Since the molecular dynamics simulations can only probe local and relatively small changes in the structure, we also manually introduced structural changes guided by knowledge of preferred cluster configurations. For this reason we cannot claim to perform global minimization of the UO_{2+x} structure. Nevertheless, a large set of possible structures was investigated and the end result should be rather close to the minimum energy ones. The molecular dynamics simulations used a lower accuracy level than the static DFT calculations. The single Γ point was applied for k space integration, and the plane wave cutoff was lowered to 300 eV.

The oxidation energy of UO_{2+x} is defined as the energy associated with the $(1/x)UO_2 + (1/2)O_2 \rightarrow (1/x)UO_{2+x}$ reaction (ΔE_O). The energy of the reference O_2 molecule was calculated by placing an isolated molecule inside a large supercell and relaxing the geometry. Since DFT within the LDA formulation is known to overestimate the binding energy of many molecules, one should apply a correction term to compensate for this. The overbinding of the O_2 molecule is about 2.4 eV;[42,59] however DFT calculations of the oxidation energy also suffer from uncertainties regarding the incorporation of oxygen into the UO_2 lattice. Here it was estimated by comparing the calculated oxidation energy of the most stable U_4O_9 structure (1.36 eV, see Section 4.1) to the experimental value of 1.8 eV.[60] This gives a correction of 0.44 eV per atom.[61] The UO_{2+x} formation energy per atom with respect to UO_2 and U_3O_8 was also applied as a measure of the stability of UO_{2+x} phases; $\Delta E_f(UO_{2+x}) = (E(UO_{2+x}) - aE(UO_2) - bE(U_3O_8))/(3 + x))$, where a and b are determined to match the UO_{2+x} nonstoichiometry. The relaxed orthorhombic α-U_3O_8 phase was used as reference, though the hexagonal form of this phase was very close in energy to the orthorhombic phase. In both cases the symmetry was slightly lowered compared to experiments during relaxation. The DFT calculations predict coexisting U^{5+} and U^{6+} ions in U_3O_8, which leads to unique crystallographic sites. The symmetry reduction is related to specific ordering of these charge-compensating U^{5+} and U^{6+} ions. Experimentally, the difference between the U sites in α-U_3O_8 is very small, and based on analysis of bonding geometries there is no evidence for independent U^{6+} ions. From this the DFT calculations seem to suggest a higher degree of charge localization than experiments. The resolution of these issues is, however, beyond the scope of the present work. The calculated volume of the U_3O_8 compound was close to experimental measurements (theory; 166.28 Å^3 and experiment; 166.49 Å^3 per formula unit[13]). The low-symmetry solution (Jahn−Teller distorted) was used as reference for UO_2. The volume of UO_2 was predicted to be 40.36 Å^3 compared to 40.87 Å^3 in experiments.[8]

3. UO_{2+X} AND U_3O_{8-Y} STRUCTURAL MODELS

Two different structural models have been used to investigate the oxidation of UO_2. In the first model extra oxygen ions are placed in the 2 × 2 × 2 fluorite supercell. On the basis of earlier experience, we focused our efforts on the split quad-interstitial cluster by adding between one and six quad-interstitial clusters in the 2 × 2 × 2 supercell. We investigated different internal arrangements of these clusters, for example, collinear or orthogonal alignment, and for some cases we also removed or added oxygen ions to study the possibility of forming clusters containing a different number of oxygen ions, such as the cuboctahedral clusters that contain five adventitious oxygen ions instead of four for the quad-interstitials. As a reference,

dx.doi.org/10.1021/ic400118p | Inorg. Chem. 2013, 52, 2769−2778

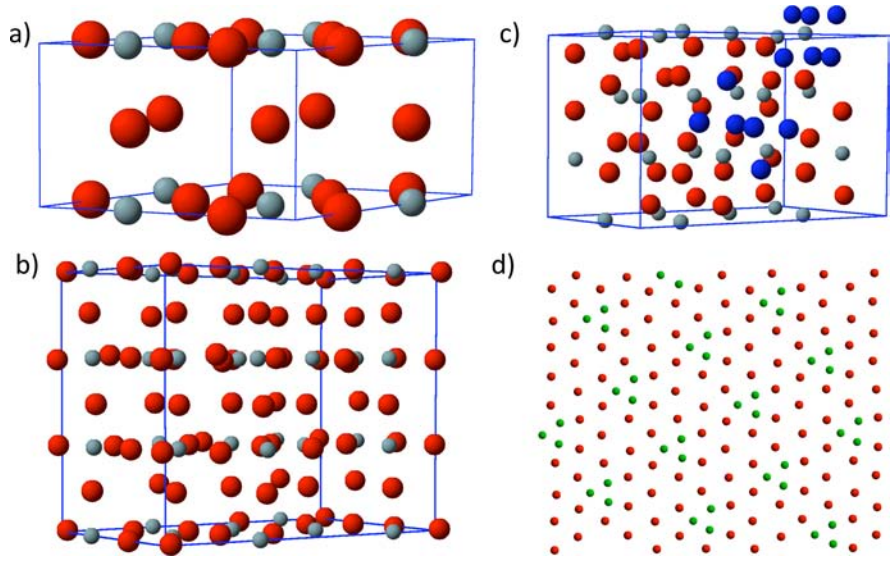

Figure 2. In all figures red spheres represent regular oxygen ions and gray spheres uranium ions. (a) The DFT relaxed unit cell of hexagonal α-U_3O_8.[62] (b) The $1 \times 2 \times 3$ supercell of α-U_3O_8 containing four vacancies.[62] The z axis in the unit cell is along the fluorite [111] direction, and the x and y axis are along [0 1 −1] and [1 −1 0] fluorite directions, respectively. (c) The structure obtained from (b) by reducing c/a to that expected for fluorite UO_2 and performing molecular dynamics annealing.[62] To better visualize the clusters (highlighted in blue) the cluster constituents were expanded beyond the unit cell boundary. Note that the corresponding cluster ions are not shown within the unit cell, but rather translated outside the cell for improving visualization. (d) Illustration of the ordering of triangular di-interstitial clusters (highlighted in green) on one of the fluorite {111} planes. This plane was cut from the $U_3O_{7.333}$ structure in (b).

single isolated interstitials and split di-interstitials (the most stable di-interstitial cluster) were also considered. The $2 \times 2 \times 2$ supercell and some of the most stable structures as a function of oxygen nonstoichiometry are illustrated in Figure 1. See also ref 62 for additional structure information.

The second UO_{2+x} structural model can be motivated from two different perspectives; (1) the structural relation between fluorite UO_2 and α-U_3O_8 that was originally derived by Allen et al.[13] or (2) the description of UO_{2+x} compounds as di- or quad-interstitial clusters of oxygen ions ordered on fluorite {111} planes proposed by Andersson et al.[19] Viewed along ⟨111⟩ directions the fluorite lattice is a stacking of uranium and oxygen planes according to the "-U-O-O-U-O-O-U-O-O-" sequence. The uranium ions in the fluorite lattice form a face centered cubic (fcc) sublattice and, consequently, the uranium planes along ⟨111⟩ directions are stacked according to the regular "-a-b-c-" fcc pattern. The α-U_3O_8 phase is related to the fluorite lattice by expanding the distance between uranium planes in the ⟨111⟩ direction and then performing a shear transformation that aligns the U sites along with rearrangement of the oxygen ions and addition of new ones, including those bridging the U ions, to reach the U_3O_8 composition. The {111} in-plane uranium−uranium coordination is almost identical between fluorite UO_2 and α-U_3O_8, while the stacking sequence is changed from "-a-b-c-" to "-a-a-a-". More details regarding this transformation can be found in refs 8, 13. At low temperature α-U_3O_8 is orthorhombic, but at high temperature it can be described by a simpler hexagonal unit cell.[8] The two models are similar and when full relaxations are included DFT calculations predict almost degenerate energies. In the DFT calculations there are slight distortions from the orthorhombic and hexagonal symmetries related to ordering of U^{5+} and U^{6+} ions. By using supercells derived from α-U_3O_8 that contain integer multiples of three uranium planes it is possible to describe both UO_2 and α-U_3O_8 within the same supercell. The only difference is the c/a ratio of the supercell. In this work supercells were derived from the hexagonal α-U_3O_8 unit cell.

To demonstrate this relation we simulated the transition from U_3O_{8-y} to UO_{2+x} by creating four oxygen vacancies in a $1 \times 2 \times 3$ supercell of hexagonal α-U_3O_8 (62 atoms), which corresponds to $U_3O_{7.333}$, and then reducing the c/a ratio to the value representative of fluorite UO_2. After this the structure was annealed according to the procedure outlined in the Section 2. Figure 2 shows the α-U_3O_8 supercell, the initial vacancy-containing α-U_3O_8 structure, and the structure obtained after reducing the c/a ratio and performing the annealing procedure. See also ref 62 for additional structure information. After relaxation the fluorite UO_{2+x} structure is recovered and instead of vacancies in α-U_3O_8 there are clusters of interstitial oxygen ions, which we identify as two separate split quad-interstitials. This cluster was previously found to be the most stable isolated cluster configuration in UO_{2+x} at 0 K using the same type of DFT calculations as applied here.[19,20]

The size of the α-U_3O_8 supercells can be modified to study different oxygen nonstoichiometries as well as different internal cluster configurations. Reduction of U_3O_8 (U_3O_{8-y}) was primarily modeled with a $1 \times 2 \times 3$ α-U_3O_8 supercell, but to investigate the low vacancy concentration regime (low y) $2 \times 2 \times 3$ (131 atoms) and $2 \times 3 \times 3$ (197 atoms) supercells were also used. The most stable U_3O_7 compound required a $2 \times 2 \times 3$ supercell (120 atoms), while the lowest energy U_4O_9 compound that we performed calculations on was described by the $2 \times 3 \times 3$ α-U_3O_8 supercell (174 atoms). The latter structure can also be captured in a much smaller primitive cell containing 58 atoms. To study variants of this U_4O_9 structure we employ expansions of the primitive cell with small shifts in the long-range periodicity accounting for changes in the internal cluster orientations, which also lead to slightly different U_4O_{9-y} nonstoichiometries. Note that we limit our search for UO_{2+x} compounds to the "-a-b-c-" stacking pattern, that is, the quad-interstitials repeat for every third uranium layer along the

dx.doi.org/10.1021/ic400118p | Inorg. Chem. 2013, 52, 2769−2778

[111] direction. Other options are possible but beyond the scope of the present investigation because of the large number of ordering possibilities that are very challenging to probe with DFT methods. Finally, calculations were performed on the experimental β- or closely related α-U_4O_9 structure described in a rhombohedral unit cell (414 atoms).

4. RESULTS AND DISCUSSION

4.1. UO_{2+x} and U_3O_{8-y} Formation Energies. Figure 3 plots the UO_{2+x} formation energy measured with respect to

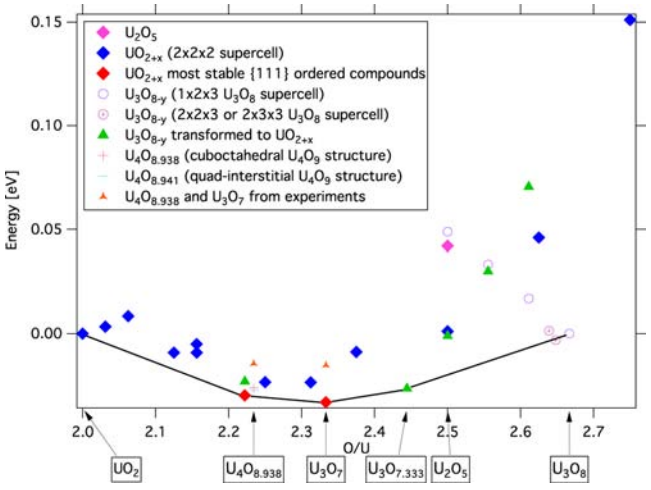

Figure 3. UO_{2+x} formation energy with respect to UO_2 and U_3O_8. UO_{2+x} refers to results obtained in the 2 × 2 × 2 supercell. From left to right the data points correspond to UO_2, a single interstitial, a split di-interstitial, a split quad-interstitial, a cuboctahedral cluster and a transformed cuboctahedral cluster (lower in energy), two split quad-interstitials, two transformed cuboctahedral clusters, three split quad-interstitials (transformed into a more complex arrangement), four split quad-interstitials, five split quad-interstitials (transformed into a more complex arrangement) and six split quad-interstitials (transformed into a more complex arrangement). UO_{2+x} {111} refers to the most stable stacking of split quad-interstitials for U_4O_{9-y} and U_3O_7 that we were able to find. U_3O_{8-y} refers to the 1 × 2 × 3 supercell of α-U_3O_8 with one, two, three, or four oxygen vacancies or to the 2 × 2 × 3 or 2 × 3 × 3 supercells of α-U_3O_8 containing one oxygen vacancy. U_3O_{8-y} transformed to UO_{2+x} refers to the fluorite compounds obtained from the 1 × 2 × 3 supercell of α-U_3O_8 supercell by contracting the c/a ratio and annealing the structure. The $U_4O_{8.938}$ and $U_4O_{8.941}$ labels refer to the DFT relaxed experimental U_4O_{9-y} structure and the most stable configuration of quad-interstitials at the exact nonstoichiometry reported for the experimental β-U_4O_{9-y} phase, respectively. The experimental data points were taken from ref 65.

UO_2 and α-U_3O_8. The different UO_{2+x} structural models, that is, the 2 × 2 × 2 fluorite supercell, the 1 × 2 × 3 α-U_3O_8 supercell (both with fluorite and U_3O_8 c/a ratio), the larger α-U_3O_8 supercells used for the lowest energy U_4O_{9-y} and U_3O_7 compounds, the cuboctahedral $U_4O_{8.938}$ and quad-interstitial $U_4O_{8.941}$ structures, are identified by unique symbols. Even though there is some scatter between the data points, which is presumably related to variation in the detailed structure such as the distribution of vacancies in U_3O_{8-y} or clusters in UO_{2+x}, we can identify several clear trends.

The convex hull along the UO_2–U_3O_8 series is spanned by UO_2, U_4O_{9-y} ($U_4O_{8.889}$), U_3O_7, $U_3O_{7.333}$, and U_3O_8. The U_4O_{9-y} and U_3O_7 phases also appear in experimental phase diagrams,[13] while $U_3O_{7.333}$ has not been reported. However, it lies between U_8O_{19} and U_2O_5, both of which have been found in experiments.[13,63] The fact that the first stable compound in the UO_{2+x} series is U_4O_{9-y} agrees with the experimentally observed phase separation of UO_{2+x} into UO_2 and U_4O_{9-y} at low temperature. Experimental phase diagrams list the composition of U_4O_{9-y} as y = 0.0588 or $UO_{2.235}$,[64] which differs from y = 0.111 or $UO_{2.222}$ obtained from DFT calculations. Figure 3 shows that both the cuboctahedral $UO_{2.234}$ ($U_4O_{8.938}$) and quad-interstitial $UO_{2.235}$ ($U_4O_{8.941}$) structures that almost exactly match the nonstoichiometry obtained in experiments are above the convex hull at 0 K and thus not predicted to be stable. The quad-interstitial $U_4O_{8.941}$ structure is slightly more stable than the cuboctahedral structure, but the difference is small. These quad-interstitial U_4O_{9-y} and U_3O_7 phases are illustrated in Figure 5, and $U_3O_{7.333}$ is shown in Figure 2. Figure 3 also includes the experimental formation energies for U_4O_{9-y} and U_3O_7,[65] which are both higher (less negative) than the calculated data, while they agree with the trend established in the calculations.

The $U_3O_{7.333}$ fluorite compound is predicted to be a stable phase between U_3O_7 and U_3O_8. The $U_3O_{7.333}$ composition is close to U_2O_5. The latter has been reported in some experiments, though, this phase is typically only formed under special synthesis conditions.[4,13] To compare these two phases we calculated the stability of δ-U_2O_5, which is the only U_2O_5 phase for which detailed crystallographic information can be found.[66] From Figure 3 it is clear that we predict U_2O_5 to be above the U_3O_7 and U_3O_8 tie line, and it is also less stable than $U_3O_{7.333}$. δ-U_2O_5 belongs to U_3O_{8-y} family, and the U_2O_5 formation energy is close to that predicted for the U_3O_{8-y} series. The fact that it is slightly lower in energy than the U_3O_{8-y} compound of the same oxygen content can probably be explained by more efficient long-range ordering of the oxygen vacancies in U_2O_5. See ref 62 for information regarding the structure of our U_3O_{8-y} derived U_2O_5 compound as well as the corresponding fluorite phase with reduced c/a ratio. δ-U_2O_5 is obviously not a thermodynamically stable compound. According to Allen et al.[13] there are also fluorite derived versions of the U_2O_5 phase (γ-U_2O_5), which would agree with the calculated phase relation in Figure 3. A phase of the U_8O_{19} composition has also been reported.[13]

The 2 × 2 × 2 supercell data set is always above the convex hull and thus less stable than the ordered U_4O_{9-y} and U_3O_7 compounds, which is expected for the low temperature phase diagram. Close to the $UO_{2.125}$ composition we see that the split quad-interstitial is predicted to be more stable than the cuboctahedral cluster at 0 K. The transformed cuboctahedral cluster that shares most of its features with the quad-interstitial cluster but has one more interstitial oxygen ion (five ions compared to four for the quad-interstitial) has a formation energy that is rather close to the quad-interstitial. Comparing the stability of the single cuboctahedron and quad-interstitial in the 2 × 2 × 2 supercell with the most stable ordered configurations at $UO_{2.234}$ ($U_4O_{8.938}$) and $UO_{2.222}$ ($U_4O_{8.889}$) we conclude that there is a significant contribution from long-range ordering for both of these defects as the individual defects are well above the convex hull. According to our calculations the quad-interstitial $U_4O_{8.889}$ phase is the most stable U_4O_{9-y} compound.

The formation energies calculated for the 2 × 2 × 2 UO_{2+x} structure models exhibit a change in slope at U_2O_5. When the data points for the ordered UO_{2+x} compounds are also considered the change in slope occurs already at $U_3O_{7.333}$.

dx.doi.org/10.1021/ic400118p | Inorg. Chem. 2013, 52, 2769–2778

This is related to change in the charge compensation mechanism from only U^{5+} ions to a combination of U^{5+} and U^{6+} ions. When the oxygen content in UO_{2+x} is large enough to require U^{6+} ions as charge compensating species the fluorite lattice is immediately destabilized with respect to U_3O_{8-y}. The opposite relation is valid for the disappearance of the U^{6+} ions in U_3O_{8-y}. In fact, according to Figure 3 a two-phase region opens up at $U_3O_{7.333}$, thus destabilizing fluorite UO_{2+x} and instead favoring nearly stoichiometric U_3O_{8-y}. $U_3O_{7.333}$ is the last compound that contain a mixture of U^{4+} and U^{5+} ions in our simulations. However, it is not until after U_2O_5 that the U_3O_{8-y} phase reaches either the same or lower formation energy than the corresponding fluorite phase of the same composition. For the highly oxidized UO_{2+x} compounds the fluorite lattice tries to prevent formation of U^{6+} ions by creating peroxide ions (O_2^{2-}). This is illustrated in Figure 1f for $UO_{2.625}$. The fact that U^{6+} ions strongly favor the layered U_3O_8 structure over the fluorite structure is related to the preference for trans-dioxo oxygen coordination of the U^{6+} ions that cannot be achieved in the fluorite lattice where the U ions have a cubic environment.

Formation of vacancies in U_3O_8 is an endothermic process (with O_2(g) as the reference state) and, consequently U_3O_8 should only exhibit limited deviation from perfect stoichiometry in the substoichiometric range and only at relatively high temperatures. The first ($U_3O_{7.944}$) and second ($U_3O_{7.917}$) U_3O_{8-y} data points in Figure 3 correspond to vacancy formation energies of 0.76 and 1.54 eV, respectively. See ref 62 for more information regarding the structure of $U_3O_{7.944}$. The slope of the formation energy curve for the remaining U_3O_{8-y} compounds is fairly constant up to the U_2O_5 stoichiometry, which is equivalent to a constant vacancy formation energy of 2.24−2.47 eV. It is visible as a linear dependence of the formation energy on the U/O ratio for the U_3O_{8-y} series in Figure 3. As reference we have also calculated the U_3O_8 reduction thermodynamics based on formation of fluorite UO_{2+x} compounds instead of U_3O_{8-y}. If reduction of U_3O_8 implies formation of $U_3O_{7.333}$ the equivalent vacancy formation energy is 0.97 eV. According to our calculations $U_3O_{7.944}$ is more stable than U_3O_8+$U_3O_{7.333}$, while all other U_3O_{8-y} compounds are less favorable than the two-phase mixtures. Experimental measurements of the vacancy formation energy energy give a value between 0.79 and 1.10 eV.[67] The first data point ($U_3O_{7.944}$) agrees well with the experimental data, while the second point ($U_3O_{7.917}$) is a bit higher than experiments. For even higher y the calculated vacancy formation energies are much higher than experiments, supporting the conclusion that these compounds are not stable.

4.2. UO_{2+x} and U_3O_{8-y} Volumes. Figure 4 plots the volume per uranium atom of the fluorite compounds in Figure 3 and Table 1 lists the volumes of some of the most important UO_{2+x} compounds. For UO_{2+x} the volume decreases linearly up to the U_2O_5 breakpoint, after which U^{6+} ions are required to achieve complete charge compensation and the volume per uranium atom starts to increase. The lattice parameter or volume decrease has been verified experimentally up to U_4O_9.[13] This decrease continues to β-U_3O_7, while the lattice parameter increases for the α-U_3O_7 polymorph.[13]

The volume of the relaxed cuboctahedral β-U_4O_9 structure stands out from the other data points by being noticeably lower. The reason for this is not clear to us, but it is another indication that long-range interactions and ordering are important factors for stabilizing the cuboctahedral geometry

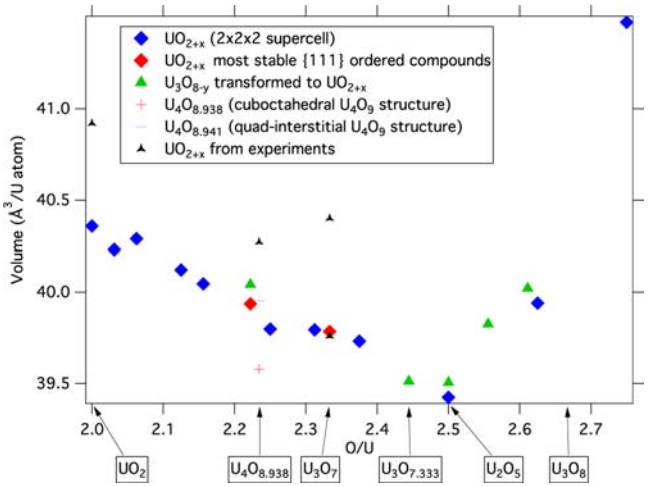

Figure 4. Volume per uranium atom for the UO_{2+x} compounds in Figure 3. The experimental data points were taken from Allen et al.[13] (see also Table 1 for more details).

in U_4O_{9-y}. The low atomic volume of the cuboctahedral U_4O_{9-y} structure indicates that it accommodates the strain induced by the oxygen ions very efficiently. The increase in volume for α-U_3O_7 compared to U_4O_{9-y} in experiments[13] (see Table 1) suggests that emergence of global strain is becoming an important factor at the U_3O_7 stoichiometry, which is also evident from the tetragonal distortion of these compounds. The increase of the atomic volume beyond the U_2O_5 break point is related to the unfavorable coordination of U^{6+} ions in the fluorite lattice.

4.3. Analysis of Cluster Ordering Patterns in U_4O_{9-y}, U_3O_7, and $U_3O_{7.333}$. The most stable U_4O_{9-y} ($U_4O_{8.889}$) and U_3O_7 compounds predicted by our calculations are illustrated in Figure 5. They can be rationalized as stacking of split quad-interstitial clusters (or equivalently the split di-interstitial clusters that make up each quad-interstitial cluster) along one of the fluorite ⟨111⟩ directions. Of the two split di-interstitial clusters that make up the larger cluster one is situated above and one below the native {111} uranium plane. Figure 5(c) and (f) show the ordering of the triangular di-interstitial clusters on these {111} oxygen planes. The DFT calculations show that the formation of ordered UO_{2+x} compounds is controlled by strong local attractive interactions between interstitial oxygen ions leading to the formation of split quad-interstitials,[19] repulsion between these clusters at close distances, and attraction at larger separations that is related to minimizing overall lattice strain and electrostatic interactions. The latter two properties are closely coupled to the distribution of U^{5+} ions on the cation sublattice. Clearly, the preferred separation between clusters is governed by the UO_{2+x} nonstoichiometry.

For U_3O_7, close to optimal packing can be achieved within the $2 \times 2 \times 3$ α-U_3O_8 supercell (Figure 5). The individual split quad-interstitials are rotated with respect to the nearest neighbor ones to maximize their internal separation. Increasing the in-plane separation of quad-interstitial clusters in the U_3O_7 structure by one step or a subset of them by two steps yields compounds close to the U_4O_9 composition. There are a several different ways to increase the distance between the clusters and each one leads to slightly different unit cells and orientation of the clusters. We have investigated a range of different possibilities. Out of these the most stable structure can be described within the $2 \times 3 \times 3$ α-U_3O_8 supercell. This structure

dx.doi.org/10.1021/ic400118p | Inorg. Chem. 2013, 52, 2769−2778

Table 1. Oxidation Energy with Respect to O_2(gas) (ΔE_O), the Formation Energy with Respect to UO_2 and U_3O_8 (ΔE_f), and the Atomic Volume (V) for the Most Important UO_{2+x} and U_3O_{8-y} Compounds[a]

	ΔE_O (eV/O atom)	ΔE_f (eV/atom)	V (Å^3/U atom)	V exp.[13] (Å^3/U atom)
UO_2	0.00	0.00	40.36	40.92
$UO_{2.222}/U_4O_{8.889}$ (quad-interstitial)	−1.80	−0.030	39.94	
$UO_{2.235}/U_4O_{8.941}$ (quad-interstitial)	−1.74	−0.027	39.92	
$UO_{2.25}/U_4O_9$ (quad-interstitial)	−1.67	−0.023	39.80	
$UO_{2.234}/U_4O_{8.938}$ (cuboctahedral)	−1.73	−0.026	39.58	40.27
$UO_{2.333}/U_3O_7$ (quad-interstitial)	−1.70	−0.033	39.78	40.40 (α-U_3O_7), 39.76 (β-U_3O_7)
$UO_{2.444}/U_3O_{7.333}$ (quad-interstitial)	−1.57	−0.026	39.51	
$UO_{2.648}/U_3O_{7.944}$	−1.39	−0.003	55.59	
$UO_{2.667}/U_3O_8$	−1.50	0.00	55.47	55.50

[a]The quad-interstitial and cuboctahedral labels denote the cluster type that the corresponding phases contain. The experimental volumes tabulated by Allen et al.[13] are also listed.

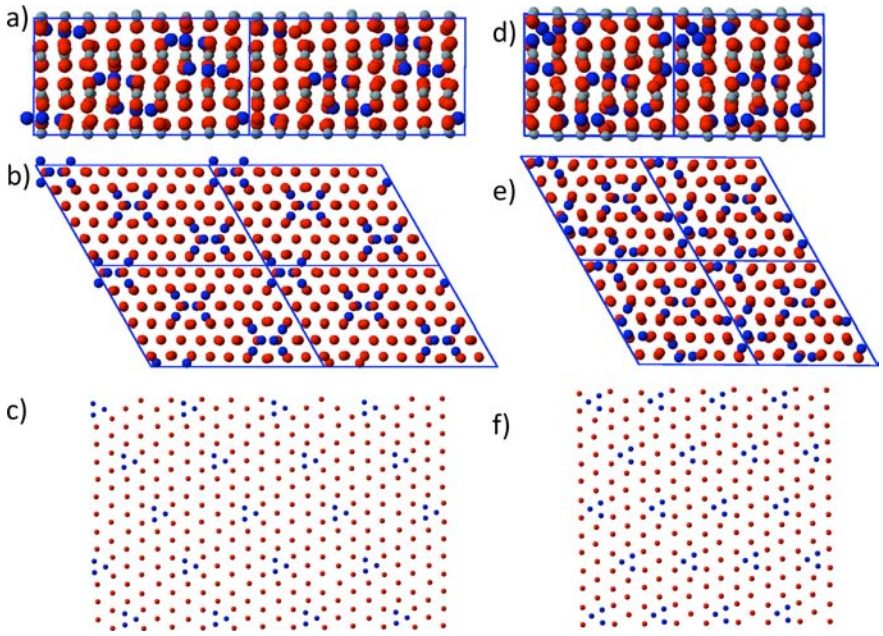

Figure 5. Lowest energy structures of U_4O_{9-y} ($U_4O_{8.889}$) (a, b, c) and U_3O_7 (d, e, f) obtained from DFT.[62] In all figures red spheres represent regular oxygen ions and gray spheres uranium ions. The cluster ions are highlighted in blue. The viewing direction in panels a and d is along the basal plane diagonal of the respective unit cells with the fluorite ⟨111⟩ direction perpendicular to this direction. In panels b and e the viewing direction is along the fluorite ⟨111⟩ direction. The oxygen clusters are stacked on the {111} planes that are perpendicular to this direction. The stacking in each {111} plane is illustrated in panels c and f.

is illustrated in Figure 5 and the composition is $UO_{2.222}$ or $U_4O_{8.889}$. It is also possible to describe the same structure within a primitive cell containing 18 uranium ions and one quad-interstitial cluster. The main difference compared to U_3O_7 is that the split quad-interstitials are further separated and aligned in the same direction.

The fact that the clustering and stacking rules outlined above are best fulfilled at the U_4O_{9-y} and U_3O_7 compositions explain why these occur as line compounds in the phase diagram. In particular these models suggest that the most stable U_4O_9 compound should be nonstoichiometric, while U_3O_7 should be very close to exact stoichiometry. In fact, experiments have established the lower oxygen limit of U_4O_{9-y} to be U/O = 2.235,[64] which is close but not identical to the composition of the structure in Figure 5. It is possible to create a quad-interstitial based structure that exactly fulfills the U/O = 2.235 criteria by rotating one of the quad-interstitials in the $UO_{2.222}$ structure and adjusting the long-range stacking accordingly. This structure is illustrated in Figure 6. However, this $UO_{2.235}$ ($U_4O_{8.941}$) structure is less stable than $UO_{2.222}$ (see Figure 3). Measured by the oxidation energy per adventitious oxygen ion the difference is about 0.05 eV. Nevertheless, the $UO_{2.235}$ structure is the second most stable quad-interstitial U_4O_9 structure that we were able to find. Bevan showed that the U/O = 2.235 nonstoichiometry is obtained almost exactly for the β-U_4O_{9-y} structure based on cuboctahedral clusters (U/O = 2.234). According to our calculations this phase is less stable than the quad-interstitial based $UO_{2.222}$ and $UO_{2.235}$ phases. Measured by the oxidation energy per atom the differences are 0.07 and 0.02 eV, respectively. U_3O_7 is often reported to be stoichiometric, but some nonstoichiometric phases have also been identified around this composition.[6,13,68]

Just as the optimally packed U_4O_{9-y} compound is related to U_3O_7 by increasing the cluster separation by one or two steps, the $U_3O_{7.333}$ compound is related to U_3O_7 by decreasing the in-plane cluster separation by one step.

At 0 K the ordering of oxygen clusters is closely coupled to the ordering of U^{4+} and U^{5+} ions, as illustrated for U_3O_7 in

dx.doi.org/10.1021/ic400118p | Inorg. Chem. 2013, 52, 2769−2778

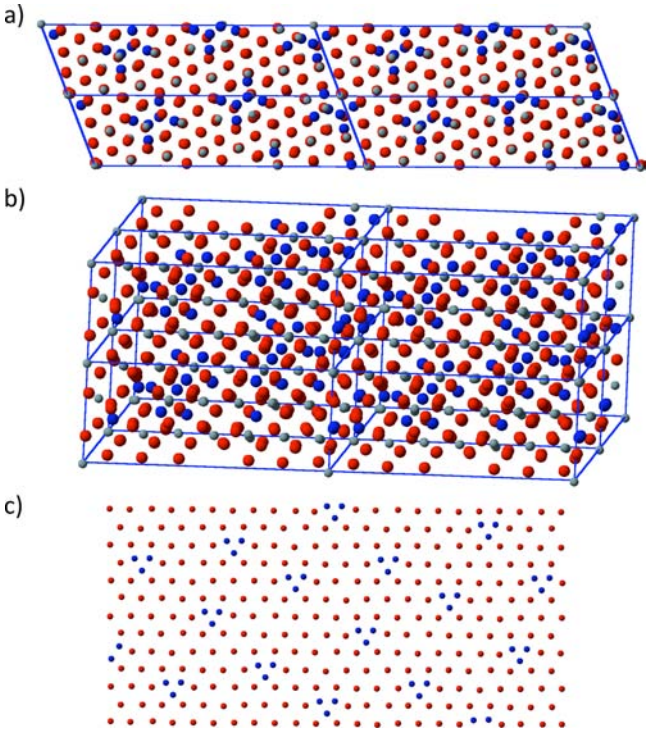

Figure 6. (a) Quad-interstitial based $UO_{2.235}$ ($U_4O_{8.941}$) structure.[62] The viewing direction in panel a is along the fluorite ⟨111⟩ direction. The oxygen clusters are stacked on the {111} planes that are perpendicular to this direction. In panel b the viewing direction is within the {111} plane perpendicular to the ⟨111⟩ direction in panel a. The stacking in each {111} plane is illustrated in panel c.

Figure 7. For this case the larger U^{4+} ions occupy the sites with the most available space and, correspondingly, the U^{5+} ions

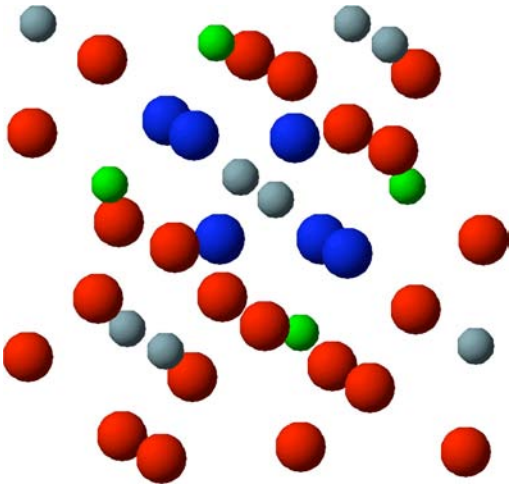

Figure 7. Green spheres show the location of U^{4+} ions in relation to the quad-interstitial cluster in the most stable U_3O_7 compound. The gray spheres represent the majority U^{5+} ions.

occupy sites with least available space, thus decreasing the strain in the system. Coulomb interactions between the charged species also influence the detailed ordering pattern and the final state should represent an optimal balance between these two contributions. It is obvious that at finite temperature the defect interactions controlling the ordering pattern at 0 K will be counteracted by entropy effects that are beyond the scope of the present work. The existence of multiple U_4O_{9-y} and U_3O_7 polymorphs as function of temperature could be a direct consequence of disordering the U^{5+}/U^{6+} ions or the cluster distribution/orientation.

4.4. Comparison of DFT Derived U_4O_{9-y} and U_3O_7 Structures with Neutron Diffraction Data. Diffraction experiments are ideal for testing the long-range ordering of oxygen clusters, whereas EXAFS and pair distribution function (PDF) analysis are more suitable for investigating the short-range order within the clusters. The crystallography of especially the low temperature phases of U_4O_9 and U_3O_7 has been an outstanding problem, mostly because of superlattice peaks that reflect unit cell multiplication and therefore defect ordering over many unit cells. Insofar as this report specifically addresses both the structure of individual defect clusters and their long-range ordering its predictions can be tested by calculating the structure factors for the various structural models and comparing them with existing experimental data. Figure 8 compares the calculated diffraction patterns with available experimental data[8] for the most stable ($U_4O_{8.889}$), the second most stable ($U_4O_{8.941}$), and the bcc cluster ordered U_4O_9[19] quad-interstitial U_4O_{9-y} phases as well as for the U_3O_7 and $U_3O_{7.333}$ phases. For U_4O_{9-y} the experimental data from Desgranges et al. were taken at 1.5 K (not yet published), while for U_3O_7 the temperature was 483 K.[8] The figure also includes calculated diffraction patterns for the DFT relaxed cuboctahedral $U_4O_{8.938}$ structure and the Rietveld refinements to the experimental data.

For the U_4O_{9-y} diffraction pattern the region most sensitive to the ordering of adventitious oxygen ions is between 28° and 36° (2θ). The Rietveld refinement shows that the low temperature data is best described by distorted cuboctahedral clusters, which include the short U−O bonds that were found in recent PDF experiments.[14,16] The DFT relaxed cuboctahedral $U_4O_{8.938}$ structure also contains distorted cuboctahedral clusters, and it agrees rather well with the experimental data, even though it does not match the data as well as the Rietveld refined model. The appearance of short U−O bonds in PDF experiments was related to an increase in the formal valence of U ions, that is, the formation of U^{6+} ions.[14,16] However, the static DFT calculations do not give any U^{6+} ions or any short U−O bonds. The physics underlying the formation of these characteristic properties is clearly not captured in the current DFT calculations.

The quad-interstitial models predict intensities of the diffraction peaks in the 28° and 36° (2θ) range that are lower than the experimental data, which indicates a larger degree of disorder than in the experimental sample. This pattern persists for most of the quad-interstitial structures that we investigated. The exception is the bcc quad-interstitial ordered U_4O_9 structure[19] (Figure 1b), which has higher intensities. However, the peak positions are not in agreement with experimental findings. One possible explanation for this behavior is that in α- or β-U_4O_{9-y} the cuboctahdral clusters have identical nearest neighbors, while the quad-interstitial structures typically exhibit a slightly more varied distribution. In diffraction experiments this should give rise to lower intensities. Again, the bcc quad-interstitial ordered U_4O_9[19] structure has a uniform nearest neighbor distribution and, as expected, it also has higher peak intensities. Since the DFT calculations predict the quad-interstitials to be more stable at 0 K there is disagreement with the experimental measurements. At this point it is not clear if this is due to inaccuracies of the DFT

dx.doi.org/10.1021/ic400118p | Inorg. Chem. 2013, 52, 2769−2778

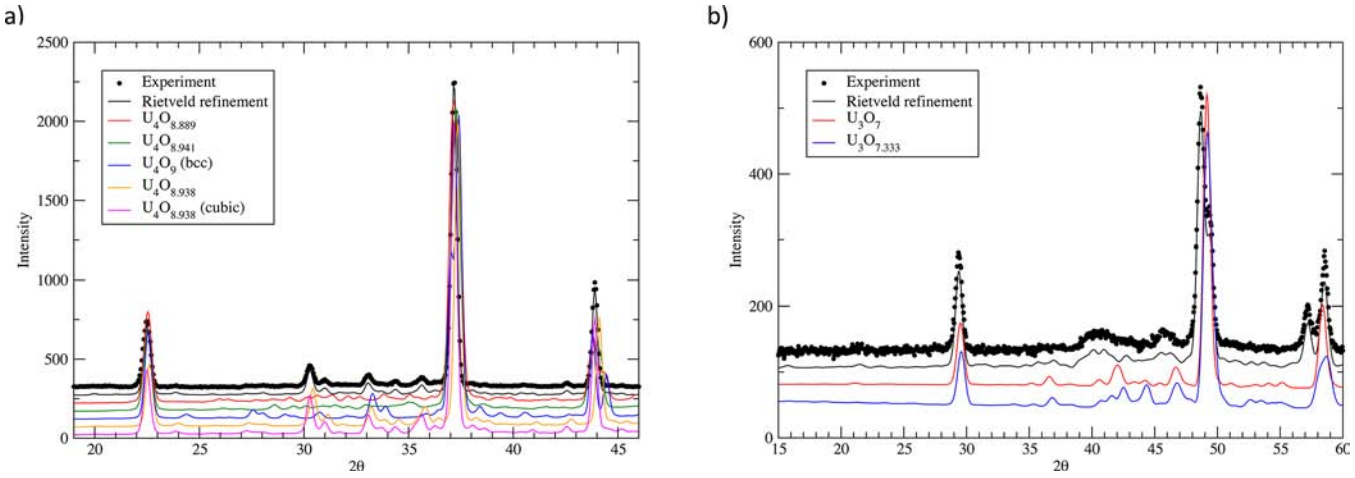

Figure 8. Calculated neutron diffraction patterns of the most stable U_4O_{9-y} (a) and U_3O_7 (b) compounds obtained from DFT compared to experimental data from Desgranges et al.[8] The experimental U_4O_9 data taken at 1.5 K has not yet been published. The experimental patterns were measured on two different diffractometers and have different wavelengths but the displayed ranges are for the corresponding region of interest: (a) λ = 1.2251 Å and (b) λ = 1.594 Å.

calculations or, for example, trapping of U_4O_{9-y} material in a β-U_4O_{9-y}-like structure because of the need for oxygen diffusion to transform into the most stable low-temperature phase.

Experimentally the U_3O_7 phase is typically distinguished from U_4O_9 by the c/a ratio deviating from unity (tetragonal distortion of the cubic cell). In the diffraction pattern in Figure 8 this is evidenced by splitting the peak between 55 and 60° (2θ), though other regions are of course also affected. Interestingly there are reports of both positive and negative splittings, that is, $c/a < 1$ and $c/a > 1$.[6] The quad-interstitial U_3O_7 model does not reproduce the deviation from cubic symmetry that is implicated by the split peak at 55−60° (2θ). Close inspection of the U_3O_7 structure obtained from calculations indicate a small shift in the c/a ratio as compared to the perfectly cubic lattice; however it is too small to reproduce the experimental diffraction data. Figure 8 also includes the diffraction pattern of the $U_3O_{7.333}$ phase, which exhibits a more significant split or broadening of this peak as well as some other peaks indicative of the tetragonal splitting. One possible explanation for the lack of c/a splitting is ordering of U^{4+} and U^{5+} ions at low temperature. The U^{4+}/U^{5+} ions occupy positions that minimize the strain in the lattice, which implies that the cubic fluorite lattice is essentially retained for U_3O_7. When the oxygen content is increased beyond U_3O_7 the balance of U^{4+}/U^{5+} ions is such that the internal strain cannot be accommodated without changing the symmetry of the lattice, which explains why $U_3O_{7.333}$ exhibits a diffraction pattern consistent with $c/a > 1$. The oxygen cluster-derived peak intensities for U_3O_7 and $U_3O_{7.333}$ are significantly higher than for the quad-interstitial U_4O_{9-y} structural models and for U_3O_7 they agree better with experiments. However, the peak positions are not in perfect agreement with experiments, which, in addition to ordering of the clusters, may be related to the lack of tetragonal splitting.

5. CONCLUSIONS

DFT calculations of UO_2 oxidation revealed stable compounds at the $U_4O_{8.889}$, U_3O_7, and $U_3O_{7.333}$ compositions, which were all based on ordering of split quad-interstitial clusters. Compounds of the same or similar compositions have been observed in experiments for the first two cases, while we could not find any reports of $U_3O_{7.333}$. The experimental U_4O_9 structure derived from ordering of cuboctahedral clusters is slightly less stable than the quad-interstitial compounds according to DFT, but the difference is rather small. The neutron diffraction patterns of the quad-interstitial U_4O_{9-y} compounds indicated a more disordered arrangement of oxygen clusters than what has been found in experiments or for the DFT relaxed version of the cuboctahedral U_4O_9 structure. The U_3O_7 structure model obtained from simulations failed to capture the tetragonal splitting revealed in experimental diffraction patterns. Reduction of U_3O_8 was investigated using similar techniques as for the oxidation of UO_2. Except for very low nonstoichiometries, U_3O_{8-y} is unstable with respect to the end-point U_3O_8 and $U_3O_{7.333}$ phases. The calculated low-temperature phase diagram shows that the fluorite derived compounds are favored up to $UO_{2.5}$, that is, as long as the charge-compensation for adding oxygen atoms occurs via formation of U^{5+} ions, after which the U_3O_{8-y} phase becomes more stable. This is also reflected in the atomic volumes of UO_{2+x} phases, which decrease up to $UO_{2.5}$ and then start increasing as soon as U^{6+} ions are formed. Even though $UO_{2.5}$ is stable with respect to U_3O_{8-y}, the upper limit of the fluorite phase boundary is at $U_3O_{7.333}$.

■ ASSOCIATED CONTENT

Ⓢ Supporting Information

Crystallographic files in cif format for the structures in Figure 1, Figure 2, and for the most stable UO_{2+x} and U_3O_{8-y} phases, that is, $U_4O_{8.889}$, $U_4O_{8.938}$, $U_4O_{8.941}$, U_3O_7, $U_3O_{7.333}$, U_2O_5 (fluorite type), U_2O_5 (U_3O_8 type) and $U_3O_{7.944}$. This material is available free of charge via the Internet at http://pubs.acs.org.

■ AUTHOR INFORMATION

Corresponding Author

*E-mail: andersson@lanl.gov.

Notes

The authors declare no competing financial interest.

■ ACKNOWLEDGMENTS

Support is acknowledged from the LDRD program at Los Alamos National Laboratory and the DOE BES Heavy Element

Chemistry program. Los Alamos National Laboratory is operated by Los Alamos National Security, LLC, for the National Nuclear Security Administration of the U.S. DOE under contract DE-AC52-06NA25396.

REFERENCES

(1) McEachern, R. J.; Taylor, P. *J. Nucl. Mater.* **1998**, *254*, 87.
(2) Olander, D. *J. Nucl. Mater.* **2009**, *389*, 1.
(3) Olander, D. R. *Fundamental Aspects of Nuclear Reactor Elements*; NTIS, ERDA, 1975.
(4) Allen, G. C.; Tempest, P. A. *Proc. R. Soc. London, Ser. A* **1986**, *406*, 325.
(5) Willis, B. T. M. *J. Chem. Soc.* **1987**, *83*, 1073.
(6) Nowicki, L.; Garrido, F.; Turos, A.; Thome, L. *J. Phys. Chem. Solids* **2000**, *61*, 1789.
(7) Cooper, R. I.; Willis, B. T. M. *Acta Crystallogr.* **2004**, *A60*, 322.
(8) Desgranges, L.; Baldinozzi, G.; Rousseau, G.; Niépce, J.-C.; Calvarin, G. *Inorg. Chem.* **2009**, *48*, 7585.
(9) Belbeoch, B.; Piekarski, C.; Perio, M. P. *J. Nucl. Mater.* **1961**, *3*, 60.
(10) Hoekstra, H. R.; Santoro, A.; Siegel, S. *J. Inorg. Nucl. Chem.* **1961**, *18*, 166.
(11) Garrido, F.; Ibberson, R. M.; Nowicki, L.; Willis, B. T. M. *J. Nucl. Mater.* **2003**, *322*, 87.
(12) Blackburn, P. E.; Weissbart, J.; Gulbransen, E. A. *J. Phys. Chem.* **1958**, *62*, 902.
(13) Allen, G. C.; Holmes, N. R. *J. Nucl. Mater.* **1995**, *223*, 231.
(14) Desgranges, L.; Baldinozzi, G.; Siméone, D.; Fischer, H. E. *Inorg. Chem.* **2011**, *50*, 6146.
(15) Bevan, D. J. M.; Grey, I. E.; Willis, B. T. M. *J. Solid State Chem.* **1986**, *61*, 1.
(16) Conradson, S. D.; Manara, D.; Wastin, F.; Clark, D. L.; Lander, G. H.; Morales, L. A.; Rebizant, J.; Rondinella, V. V. *Inorg. Chem.* **2004**, *43*, 6922.
(17) Conradson, S. D.; et al. **2012**, submitted for publication.
(18) Salkola, M. I.; Bishop, A. R.; Trugman, S. A.; Mustre de Leon, J. *Phys. Rev. B* **1995**, *51*, 8878.
(19) Andersson, D. A.; Lezama, J.; Uberuaga, B. P.; Deo, C.; Conradson, S. D. *Phys. Rev. B* **2009**, *79*, 024110.
(20) Andersson, D. A.; Espinosa-Faller, F. J.; Uberuaga, B. P.; Conradson, S. D. *J. Chem. Phys.* **2012**, *136*, 234702.
(21) Liechtenstein, A. I.; Anisimov, V. I.; Zaanen, J. *Philos. Mag.* **1995**, *52*, 5467.
(22) Kresse, G.; Joubert, D. *Phys. Rev. B* **1999**, *59*, 1758.
(23) Blöchl, P. E. *Phys. Rev. B* **1994**, *50*, 17953.
(24) Kresse, G.; Hafner, J. *Phys. Rev. B* **1993**, *48*, 13115.
(25) Kresse, G.; Furthmüller, J. *Comput. Mater. Sci.* **1996**, *6*, 15.
(26) Kresse, G.; Furthmüller, J. *Phys. Rev. B* **1996**, *54*, 11169.
(27) Prodan, I. D.; Scuseria, G. E.; Martin, R. L. *Phys. Rev. B* **2006**, *73*, 045104.
(28) Roy, L. E.; Durakiewicz, T.; Martin, R. L.; Peralta, J. E. *J. Comput. Chem.* **2008**, *29*, 2288.
(29) Petit, L.; Svane, A.; Szotek, Z.; Temmerman, W. M.; Stocks, G. M. *Phys. Rev. B* **2010**, *81*, 045108.
(30) Dudarev, S. L.; Manh, D. N.; Sutton, A. P. *Philos. Mag.* **1997**, *75*, 613.
(31) Iwasawa, M.; Chen, Y.; Kaneta, Y.; Ohnuma, T.; Geng, H. Y.; Kinoshita, M. *Mater. Trans.* **2006**, *47*, 2651.
(32) Laskowski, R.; Madsen, G. K. H.; Blaha, P.; Schwarz, K. *Phys. Rev. B* **2004**, *69*, 140408.
(33) Gupta, F.; Brillant, G.; Pasturel, A. *Philos. Mag.* **2007**, *87*, 2561.
(34) Geng, H. Y.; Chen, Y.; Kaneta, Y.; Kinoshita, M. *Phys. Rev. B* **2007**, *75*, 054111.
(35) Geng, H. Y.; Chen, Y.; Kaneta, Y.; Iwasawa, M.; Ohnuma, T.; Kinoshita, M. *Phys. Rev. B* **2008**, *77*, 104120.
(36) Geng, H. Y.; Chen, Y.; Kaneta, Y.; Kinoshita, M. *Phys. Rev. B* **2008**, *77*, 180101.
(37) Geng, H. Y.; Chen, Y.; Kaneta, Y.; Kinoshita, M. *Appl. Phys. Lett.* **2008**, *93*, 201903.
(38) Nerikar, P.; Watanabe, T.; Tulenko, J. S.; Phillpot, S. R.; Sinnott, S. B. *J. Nucl. Mater.* **2009**, *348*, 61.
(39) Dorado, B.; Amadon, B.; Freyss, M.; Bertolus, M. *Phys. Rev. B* **2009**, *79*, 235125.
(40) Brillant, G.; Pasturel, A. *Phys. Rev. B* **2008**, *77*, 184110.
(41) Dorado, B.; Jomard, G.; Freyss, M.; Bertolus, M. *Phys. Rev. B* **2010**, *82*, 035114.
(42) Andersson, D. A.; Watanabe, T.; Deo, C.; Uberuaga, B. P. *Phys. Rev. B* **2009**, *80*, 060101.
(43) Meredig, B.; Thompson, A.; Hansen, H. A.; Wolverton, C.; van de Walle, A. *Phys. Rev. B* **2010**, *82*, 195128.
(44) Hanken, B. E.; Stanek, C. R.; Grønbech-Jensen, N.; Asta, M. *Phys. Rev. B* **2011**, *84*, 085131.
(45) Thompson, A. E.; Wolverton, C. *Phys. Rev. B* **2011**, *84*, 134111.
(46) Devey, A. J. *J. Nucl. Mater.* **2011**, *412*, 301.
(47) Yun, Y.; Rusz, J.; Suzuki, M.-T.; Oppeneer, P. M. *Phys. Rev. B* **2011**, *83*, 075109.
(48) Yun, Y.; Kim, H.; Lim, H.; Park, K. *J. Korean Phys. Soc.* **2007**, *50*, 1285.
(49) Conradson, S. D.; et al. **2013**, manuscript in preparation.
(50) Geng, H. Y.; Song, H. X.; Jin, K.; Xiang, S. K.; Wu, Q. *Phys. Rev. B* **2011**, *84*, 174115.
(51) Zhou, F.; Ozolins, V. *Phys. Rev. B* **2009**, *80*, 125127.
(52) Zhou, F.; Ozolins, V. *Phys. Rev. B* **2011**, *83*, 085106.
(53) Gotoo, K.; Nomura, S.; Naito, K. *J. Phys. Chem. Solids* **1965**, *26*, 1679.
(54) Crocombette, J.-P.; Torumba, D.; Chartier, A. *Phys. Rev. B* **2011**, *83*, 184107.
(55) Crocombette, J.-P. *Phys. Rev. B* **2012**, *85*, 144101.
(56) Pireaux, J. J.; Rica, J.; Thibaut, E.; Tenret-Noel, C.; Caudano, R.; Verbist, J. J. *Chem. Phys.* **1977**, *22*, 113.
(57) Baer, Y.; Schoenes, J. *Solid State Commun.* **1980**, *33*, 885.
(58) Beatham, N.; Orchard, A. F.; Thornton, G. *J. Electron Spectrosc. Relat. Phenom.* **1980**, *19*, 205.
(59) Kurth, S.; Perdew, J. P.; Blaha, P. *Int. J. Quantum Chem.* **1999**, *75*, 889.
(60) Gueneau, C.; Baichi, M.; Labroche, D.; Chatillon, C.; Sundman, B. *J. Nucl. Mater.* **2002**, *304*, 161.
(61) Dorado, B.; Andersson, D. A.; Stanek, C. R.; Bertolus, M.; Uberuaga, B. P.; Martin, G.; Freyss, M.; Garcia, P. *Phys. Rev. B* **2012**, *86*, 035110.
(62) See Supporting Information for structure coordinates.
(63) Hoekstra, H. R.; Siegel, S.; Charpint, P. *J. Inorg. Nucl. Chem.* **1968**, *30*, 519.
(64) Van Lierde, W.; Pelsemaekers, J.; Lecocq-Robert, A. *J. Nucl. Mater.* **1970**, *37*, 276.
(65) Grenthe, I.; Fuger, J.; Konings, R. J. M.; Lemire, R. J.; Muller, A. B.; Nguyen-Trung, C.; Wanner, H. In *Chemical Thermodynamics of UO_2*; Wanner, H., Forest, I., Eds.; Nuclear Energy Agency Organization for Economic Co-Operation and Development, 2004.
(66) Kovba, L. M.; Komarevtseva, N. I.; Kuzmitcheva, E. U. *Radiokhimiya* **1979**, *21*, 754.
(67) Matsui, T.; Tsuji, T.; Naito, K. *J. Nucl. Sci. Technol.* **1974**, *11*, 317.
(68) Morss, L. R., Edelstein, N. M., Fugeri, J., Eds.; *The Chemistry of the Actinide and Transactinide Elements*, 4th ed.; Springer: New York, 2011; Vols. *1*−*6*.